Astron. Astrophys. 360, 952–968 (2000)

ASTRONOMY AND ASTROPHYSICS

The evolution of AGB stars with convective overshoot

F. Herwig

Universität Potsdam, Institut für Physik, Astrophysik, Am Neuen Palais 10, 14469 Potsdam, Germany (fherwig@astro.physik.uni-potsdam.de)
Astrophysikalisches Institut Potsdam (AIP), An der Sternwarte 16, 14482 Potsdam, Germany

Received 13 December 1999 / Accepted 15 June 2000

Abstract. The influence of extended convective mixing (overshoot) on asymptotic giant branch stellar evolution is investigated in detail. The extended mixing is treated time-dependently, and the efficiency declines exponentially with the geometric distance from the convective boundary. It has been considered at all convective boundaries, including the He-flash convection zone in the intershell region which forms during the thermal pulses.

Both the structural and the chemical evolution are affected by the inclusion of overshoot. The main results include a very efficient third dredge-up which leads to the formation of carbon stars of low mass and luminosity. A ^{13}C pocket which may serve as a neutron source for the s-process can form after the third dredge-up has reached into the ^{12}C rich intershell. Overshoot applied to the pulse-driven convective zone during the He-flash leads to a deeper penetration of the bottom of this convective zone into the C/O core below the He-burning shell. This in turn causes ^{4}He to be less abundant in the intershell while ^{12}C and ^{16}O are more abundant compared to calculations without overshoot. We show that overshoot at the He-flash convection zone as well as at the base of the envelope convection enhance the efficiency of the third dredge-up. Characteristic properties of the structural and chemical evolution of AGB stars are presented.

Key words: stars: abundances – stars: interiors – stars: evolution – stars: AGB and post-AGB

1. Introduction

Towards the end of their lifetime, stars of low and intermediate mass ($\mathrm{M} < 8\,\mathrm{M}_{\odot}$) evolve along the Asymptotic Giant Branch (AGB) stage (Iben & Renzini 1983; Habing 1996; Lattanzio & Boothroyd 1997). The core of carbon and oxygen is surrounded by a sandwich like structure consisting of a helium burning shell, the hydrogen burning shell and the intershell region in between. Evolved AGB stars undergo recurrent thermal instabilities of the helium burning shell (He-flash) which are referred to as thermal pulses (TP) (Schwarzschild & Härm 1965; Weigert 1966). Locally, helium burning peak luminosities of $\log L_{\mathrm{He}}/\,\mathrm{L}_{\odot} \simeq 5 \ldots 8$ are released and cause complex convective mixing events. The He-flash causes a pulse-driven convective zone (PDCZ) in the intershell region. After the He-flash the bottom boundary of the convective envelope may engulf the deeper regions where material previously synthesized by hydrogen and helium burning is present (third dredge-up, TDUP).

Despite many studies of AGB evolution (Iben 1976; Schönberner 1979; Lattanzio 1986; Boothroyd & Sackmann 1988a; Vassiliadis & Wood 1993; Blöcker 1995; D'Antona & Mazzitelli 1996; Forestini & Charbonnel 1997; Straniero et al. 1997; Wagenhuber & Groenewegen 1998), important details, like the surface enrichment with nuclear processed material from the deep interior (dredge-up) or the origin of ^{13}C which is an important source of neutrons for the synthesis of heavy elements in AGB stars, are not very well understood. To improve this situation we present the structural properties as well as the chemical evolution of the interior of AGB stellar models with convective overshoot. Convective motions of matter approach the convective boundary with a non-zero velocity and penetrate into the formally stable region. These overshooting flows lead to extra mixing of elements. Canuto (1998) has pointed out that overshoot is a dynamical consequence of Newton's laws and as such is unavoidable. Previous studies have shown that models with overshoot can account for several observed properties of AGB and post-AGB stars (Blöcker et al. 1997; Herwig et al. 1997, 1998, 1999b).

We give a brief review of AGB star properties relevant for our new models (Sect. 2), some remarks on the stellar evolution code as well as some information on overshoot and its treatment in our models (Sect. 3). We explain the differences between models without overshoot and with overshoot by looking separately at the two relevant convective boundaries: the bottom of the envelope convection (Sect. 4) and the bottom of the PDCZ (Sect. 5). The chemical and structural surface properties of models with overshoot are described in Sect. 6. Conclusions are presented in Sect. 7.

2. Some properties of AGB stars, stellar models, and overshoot

Carbon stars and the third dredge-up. AGB stars show a large range of surface C/O ratios from about the solar value $\simeq 0.4$ up to well above unity. In particular many low-mass AGB stars show up as carbon stars with $\mathrm{C/O} > 1$ (Smith et al. 1987; Frogel et al. 1990). Half of all planetary nebulae are carbon rich as well (Zuckerman & Aller 1986). Already the early stellar evolution calculations (Iben 1975; Iben 1977; Iben & Truran 1978; Sackmann 1980) pointed towards the TDUP to provide a

link between the intershell region where carbon is present and the bottom of the envelope convection.[1] However, these models have not shown sufficient dredge-up for AGB models with low (core) masses. Lattanzio (1989) used a method to determine the convective boundary which ensures that the ratio of radiative and adiabatic temperature gradient approaches unity smoothly at the convective boundary. This method favors the occurrence of the TDUP even for low mass stars of solar metallicities. Hollowell & Iben (1988) found for low mass and low metallicity that the dredge-up of processed material occurs if some additional mixing is assumed. Wood (1981) and Boothroyd & Sackmann (1988b) showed that lower metallicity and increased mixing length parameter enhances TDUP. Straniero et al. (1997) find the TDUP for low-mass AGB stars and relate its occurrence to increased numerical resolution. Calculations which do not find dredge-up for low core masses are the rule rather than the exception (Vassiliadis & Wood 1993; Blöcker 1995; Forestini & Charbonnel 1997; Wagenhuber & Groenewegen 1998; Langer et al. 1999). Herwig et al. (1997) presented first results of a $3\,\mathrm{M}_\odot$ stellar model sequence which had been computed with convective overshoot, treated time-dependently at all convective boundaries. With this approach TDUP was very efficient for low core masses and solar metallicity.

Intershell abundances. The abundance distribution in the intershell is of great importance because in this region the major nuclear burning and mixing processes associated with the He-flash and the TDUP take place. The intershell abundances are determined by nuclear burning during the quiescent interpulse phase (mainly hydrogen burning), the nuclear processing during the TP, the convective mixing in the pulse-driven convective zone, and third dredge-up. The intershell abundance is significantly affected if overshoot is applied to the PDCZ because additional material is mixed into the intershell from the C/O core (Sect. 5.2).

It affects the local nuclear production, the surface enrichment and also the structure of the star. It is also of relevance for the interpretation of surface abundances of hydrogen-deficient post-AGB stars (see e.g. Schönberner 1996; Iben et al. 1996 or Werner et al. 1999).

Neither Schönberner (1979) nor Boothroyd & Sackmann (1988a) considered overshoot and both found that the abundance distribution in the intershell evolves with each TP. Starting with an almost pure He composition from previous hydrogen burning at the first TP, the abundances approach typical values of (He/C/O)=(0.76/0.22/0.02) (mass fractions) after a few TPs.

^{13}C *production.* The observed correlation of s-process elements and carbon in low-mass stars (Smith & Lambert 1990) points to low-mass stars as a likely site for n-capture nucleosynthesis (Gallino et al. 1997; Wallerstein et al. 1997). Gallino et al. (1998) have demonstrated that, *if* hydrogen ingestion from the envelope into the intershell region at the end of the TDUP is assumed *then* the subsequent formation of ^{13}C via the nuclear reaction $^{12}\mathrm{C}(\mathrm{p},\gamma)^{13}\mathrm{N}(e^+\nu)^{13}\mathrm{C}$ does indeed predict a neutron exposure which leads to a s-process enhancement in compliance with the solar main component of heavy elements. However, the physical mechanism of H-ingestion is unclear. Depth-dependent overshoot naturally predicts the formation of a ^{13}C pocket as needed for the s-process nucleosynthesis.

Mixing and overshoot. Mixing of elements in stars is attributed to a number of processes (Pinsonneault 1997) of which convection is the most effective. Stellar evolution models commonly employ the mixing-length theory (MLT) (Böhm-Vitense 1958) or some descendent thereof. The boundary of convective instability is determined by the local Schwarzschild condition $\nabla_{\mathrm{rad}} > \nabla_{\mathrm{ad}}$ where ∇_{ad} and ∇_{rad} are the adiabatic and radiative gradient (Kippenhahn & Weigert 1990). However, neighboring layers are related by inertia, momentum transfer and the equation of continuity and therefore convective elements might overshoot beyond the boundary of convection (e.g. Shaviv & Salpeter 1973; Maeder 1975; Roxburgh 1978; Bressan et al. 1981; Langer 1986). No commonly accepted quantitative theoretical description of convective overshoot currently exists (Renzini 1987).

Comparison of stellar models with observational findings indicates that convective overshoot occurs in real stars (Mermilliod & Maeder 1986; Maeder & Meynet 1989; Andersen et al. 1990; Stothers 1991; Napiwotzki et al. 1991; Alongi et al. 1991; Alongi et al. 1993; Schröder et al. 1997; Kozhurina-Platais et al. 1997). Overshooting in stellar evolution calculations has been simulated by an extension of the instantaneous mixing beyond the convective boundary (instantaneous overshoot). The widely used set of models by Schaller et al. (1992) has been calculated with an overshoot distance of one fifth pressure scale height ($\alpha_{over} = 0.2$) which was calibrated in order to fit the observed terminal age main sequence of 65 stellar clusters and associations. Improving on the instantaneous treatment, Deng et al. (1996a; 1996b) and Salasnich et al. (1999)) have explored the effects of turbulent diffusion in the overshoot region of massive stars.

Due to the insights of two- as well as three-dimensional hydrodynamical simulations convection is nowadays pictured in terms of downdrafts and up-flows rather than as a hierarchy of eddies (Stein & Nordlund 1998). Two-dimensional simulations showed that prominent downward-directed plumes can overshoot a substantial distance into the stable region (Hurlburt et al. 1986; Hurlburt et al. 1994; Freytag et al. 1996). These models show emerging and vanishing patterns of curls, fast narrow downdrafts and broad up-flow regions.The turbulent velocity field decays exponentially beyond the convective boundary (see also Xiong 1985; Asida & Arnett in prep.). These results have been applied via a time-dependent treatment of convective mixing to low- and intermediate mass

[1] The third dredge-up is to be distinguished from the *first* dredge-up which occurs during the first ascent of the giant branch after central hydrogen exhaustion and the *second* dredge-up which occurs during the early AGB phase for more massive AGB stars after the end of core helium burning.

stellar models by Herwig et al. (1997; 2000) (low mass TP-AGB), Ventura et al. (1998) (main sequence) and Mazzitelli et al. (1999) and Blöcker et al. (2000) (massive AGB stars, HBB).

3. The stellar evolution code and computations

General aspects of the code. The results presented in this paper have been obtained with the stellar evolution code described by Blöcker (1995) with the modifications given in Herwig et al. (1997). Here, we will add only a few relevant details. The $^{12}\mathrm{C}(\alpha,\gamma)^{16}\mathrm{O}$ reaction rate has been taken from Caughlan & Fowler (1988) and multiplied by a factor of 1.7 as recommended by Weaver & Woosley (1993). The reaction rates $^{17}\mathrm{O}(\mathrm{p},\gamma)^{18}\mathrm{F}$ and $^{17}\mathrm{O}(p,\alpha)^{14}\mathrm{N}$ have been taken from the compilation of Landré et al. (1990) as described in El Eid (1994). The model sequence without overshoot has been computed with the latest *OPAL* opacity tables (Iglesias & Rogers 1996). This choice had purely technical reasons but does not affect the comparison.

The adjustment of the numerical resolution (geometry and time) plays an important role in the computation of AGB models (Straniero et al. 1997; Frost & Lattanzio 1996; Mowlavi 1999). The resolution is adjusted from model to model according to the changes of the state variables as a function of time and location within the star. For example, the luminosity due to nuclear processing of helium L_{He} should not change more than 5% between two models. The models have $\simeq 1900\ldots2300$ mass grid points which accumulate around the core-envelope interface where the pressure and density drop steeply. The model time steps range from about a dozen years during the quiescent H-burning interpulse phase down to typically a few days during the He-flash and the following phase where dredge-up may occur (Sect. 4.1).

Exponential diffusive overshoot. For the time-dependent treatment of overshoot mixing we follow the prescription of Freytag et al. (1996). The particle spreading in the overshoot region can be described as a diffusion process and the diffusion coefficient D_{OV} can be fitted by a formula like

$$D_{\mathrm{OV}}(z) = t_{\mathrm{c}} \cdot v^2_{\mathrm{rms}}(z) \tag{1}$$

where z denotes the geometric distance from the edge of the convective zone and t_{c} is a characteristic time scale for the considered convection zone. Combining this with the finding of an exponential decay of the velocity field, Freytag et al. (1996) give the diffusion coefficient in the overshoot region as

$$D_{\mathrm{OV}} = D_0 \exp\left(\frac{-2z}{H_{\mathrm{v}}}\right), \quad H_{\mathrm{v}} = f \cdot H_{\mathrm{p}}, \tag{2}$$

where H_{v} is the velocity scale height of the overshoot convective elements at the convective boundary. H_{v} can be expressed as a fraction f of the pressure scale height H_{p}. The quantity D_0 is the expression $v^2_{\mathrm{edge}} t_{\mathrm{c}}$ in Freytag et al. (1996: Eq. 9). Here we have approximated D_0 by the diffusion coefficient in the convectively unstable region near the convective boundary r_{edge}. Note that D_0 is well defined because D_{c} approaches the convective boundary with a small slope and drops almost discontinuously at r_{edge}. The diffusion coefficient D_{c} in the convection zone can be derived from the MLT (see Langer et al. 1985). In the radiative zone where the diffusion coefficient has dropped below $D^{\mathrm{limit}}_{\mathrm{OV}} = 1 \cdot 10^{-2}\mathrm{cm}^2/\mathrm{s}$ no element mixing is allowed ($D_{\mathrm{rad}} = 0$).

The free parameter f in Eq. (2) describes the efficiency of the extra diffusive mixing. For larger f the extra partial mixing beyond the convective edge extends further. In their simulations Freytag et al. (1996) found velocity scale heights of the order of a pressure scale height ($f \simeq 1$). However, under adiabatic conditions the convective flows move so fast that they will not be able to exchange heat efficiently with the surrounding when entering into the stable region. Accordingly a stronger deceleration of the plumes is likely in the stellar interior compared to the situation of the shallow surface convection zones. In order to obtain an order of magnitude for f in the stellar interior it has been scaled to reproduce the observed width of the main sequence. A parameter of $f \simeq 0.016$ was found to reproduce the models of Schaller et al. (1992) (see end of Sect. 2). Using AGB overshoot models as a starting point for post-AGB models of H-deficient objects has confirmed this assumption a posteriori, at least for the bottom of the He-flash convection zone (Herwig et al. 1999a).

The overshoot prescription (Eq. (2)) has been applied irrespective of μ-gradients which may decrease the overshoot efficiency (Langer et al. 1983). The analysis of old open clusters even suggests that overshoot may not expand against μ-gradients in low mass stars (Aparicio et al. 1991). Theoretically, Canuto (1998) has recently argued that μ-gradients do decrease the overshoot efficiency, but do not prevent the effect entirely. In our study, this aspect becomes important at the bottom of the envelope convection during the third dredge-up. As explained in Sect. 5.3 the results are not significantly dependent on the amount of overshoot at this convective boundary.

The stellar evolution computations. The findings in this work are based on two model sequences of $3\,\mathrm{M}_\odot$ and $4\,\mathrm{M}_\odot$ with overshoot. For comparison, one $3\,\mathrm{M}_\odot$ TP-AGB sequence has been computed without overshoot. It has been started from a $3\,\mathrm{M}_\odot$ overshoot model taken just before the occurrence of the first TP (Figs. 7, 9, 10, 15). In order to study the dependence of the evolution of the intershell abundance as a function of the parameter f a few more sequences with different f-values have been computed from this starting model (Fig. 12) and followed over three thermal pulses. In addition, the eighth TP cycle of the $3\,\mathrm{M}_\odot$ overshoot case has been recomputed for different f values (Figs. 13, 14). In Fig. 1 a recomputation of the 14^{th} TP of the $3\,\mathrm{M}_\odot$ sequence initially without overshoot is shown.

A solar-like initial composition, $(Y, Z) = (0.28, 0.02)$, has been chosen corresponding to Anders & Grevesse (1989). The mixing-length parameter of the MLT is $\alpha_{\mathrm{MLT}} = 1.7$ which has been calibrated by reproduction of the solar surface parameters. A Reimers-type mass loss with efficiency $\eta = 1$ has been ap-

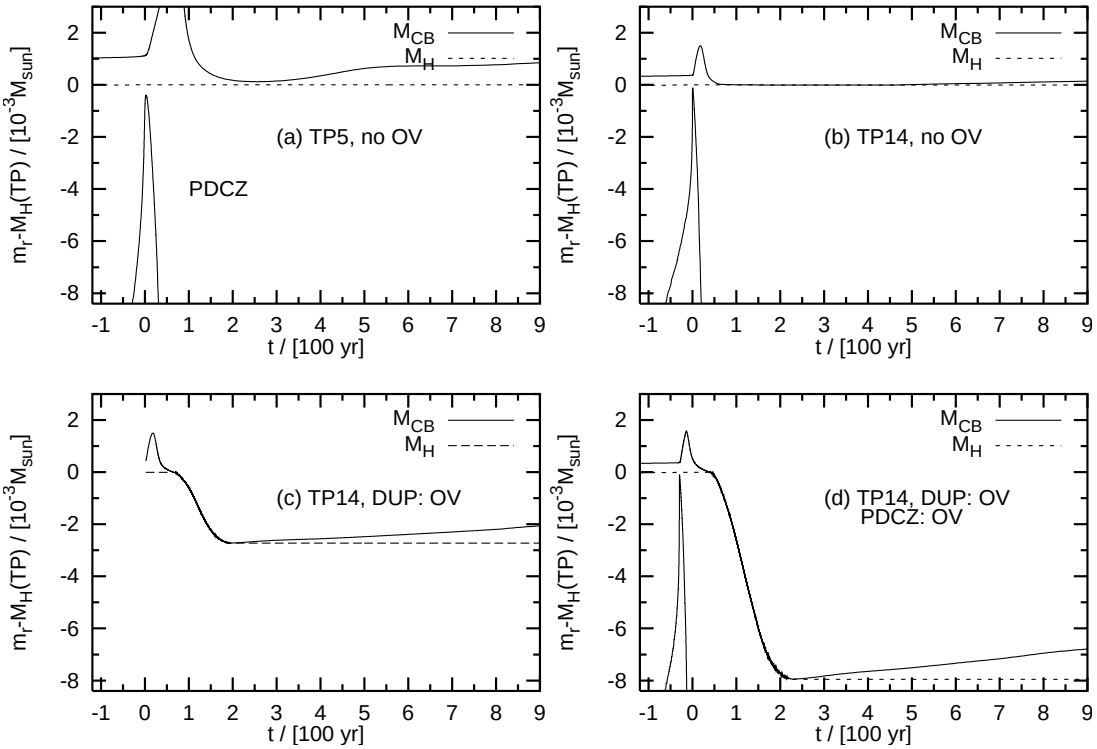

Fig. 1a–d. Evolution of mass coordinate of convective boundary ($\mathrm{M_{CB}}$, solid line) and H-free core ($\mathrm{M_H}$, dashed line). The mass scale has been set to zero at the mass coordinate of the H-free core at the time of the He-flash (TP5: $M_{\rm H} = 0.6421\,\mathrm{M}_\odot$; TP14: $M_{\rm H} = 0.6917\,\mathrm{M}_\odot$). The time scale has bee set to zero at the peak of the He-flash luminosity (TP5: $t_0 = 227034\,\mathrm{yr}$; TP14: $t_0 = 677076\,\mathrm{yr}$). The spike (solid line) at $t = 0\,\mathrm{yr}$ shown in **a**, **b** and **d** is the top of the pulse-driven convection zone of the He-flash. The upper solid line shows the bottom boundary of the envelope convection zone. Panel **a**: $5^{\rm th}$ TP of the $3\,\mathrm{M}_\odot$ sequence without overshoot; panel **b**: $14^{\rm th}$ TP of the same sequence; panel **c**: the same TP as in **b** started after the PDCZ has vanished and with overshoot at the bottom of the envelope convection zone; panel **d**: again the $14^{\rm th}$ TP recalculated from before the onset of the He-flash, with overshoot at the PDCZ and during the following TDUP episode.

plied. The Reimers mass loss formula has not been designed for AGB stars, however for the purpose of this study mass loss is not important. The $3\,\mathrm{M}_\odot$ ($4\,\mathrm{M}_\odot$) model sequence has a total mass of $2.686\,\mathrm{M}_\odot$ ($3.689\,\mathrm{M}_\odot$) at the $12^{\rm th}$ ($11^{\rm th}$) TP (see Table 1 and 2).

Overshoot has been applied during all evolutionary stages and to all convective boundaries. Overshoot applied to the main sequence core convection has indirect implications for AGB star models as it shifts the core masses at the first thermal pulse upward and decreases the progenitor mass ($M_{\rm up}$) limit for C/O white dwarfs (Alongi et al. 1993). If overshoot is also applied during the second DUP phase this effect is counterbalanced somewhat and $M_{\rm up} \simeq 6.5$ (T. Driebe, priv. com., see also Blöcker et al. (2000) and Weidemann (2000)). This is just above the value obtained from models in which overshoot is only applied during the main sequence phase (Bressan et al. 1993).

4. Overshoot at the bottom of the convective envelope

Overshoot at the bottom of the convective envelope has an effects on the modeling of the TDUP and on the formation of a ^{13}C pocket after the end of the dredge-up phase.

4.1. The third dredge-up

It has been a matter of discussion whether convective overshoot at the bottom of the convective envelope is a prerequisite for dredge-up (Mowlavi 1999). This question is closely linked to the general problem of determining the convective boundary of mixing within the framework of a local theory of convection together with its numerical implementation. As reported by previous authors (e.g. Paczyński 1977), our models without overshoot develop a discontinuity in $\nabla_{\rm rad}$ when the bottom of the envelope convection zone reaches the He-rich buffer layer. This discontinuity can prohibit the TDUP under certain conditions. In our models of AGB stars with not so massive cores the flux on the stable side of the convective boundary is not large enough to lift $\nabla_{\rm rad}$ above $\nabla_{\rm ad}$.

In Fig. 1 the situation in the dredge-up region is shown for several thermal pulses computed with different assumptions on overshoot. After an early TP of the $3\,\mathrm{M}_\odot$ sequence computed without any overshoot (panel a) the bottom of the envelope convection does not approach the H-free core close enough for any dredge-up. For more advanced TP (panel b) the convection clearly approaches the H-free core for a period of about $300\,\mathrm{yr}$ but due to the effect of the abundance discontinuity shown in Fig. 3 the lack of overshoot prohibits the TDUP. This is evident

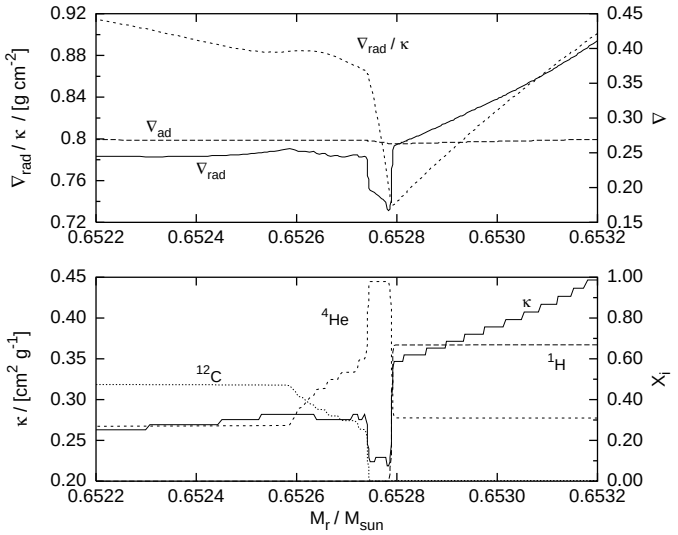

Fig. 2. Temperature gradients, opacity and abundances for the mass fraction in the AGB star during the TDUP ($f = 0.016$) after the eighth TP with overshoot. $t = 216\,\mathrm{yr}$ after peak helium luminosity. Compare Fig. 3: there the bottom of the convective envelope does not reach into the He-rich buffer zone at $M_\mathrm{r} = 0.6529\,\mathrm{M}_\odot$, whereas in the case shown here the envelope has started to engulf the He-rich buffer zone.

from panel (c) which shows the same situation with overshoot switched on below the bottom of the envelope convection. In this case a considerable dredge-up of material is possible. Panel (d) shows that overshoot applied also to the preceding PDCZ increases the DUP efficiency even further, which is discussed in detail in Sect. 5. Note that if overshoot only at the base of the convective envelope had been applied for the 5^th TP shown in Fig. 1, this would have had no effect on DUP because the stable layer between the bottom boundary of convection and the H-free core is too large compared to the tiny extent of the overshoot layer. Fig. 3 demonstrates the situation of panel (b) of Fig. 1 as a set of profiles. The bottom of the convective envelope recoils at the He-rich region which encloses the core, despite the fact that contact between the convective envelope and the H-free core is established over a few hundred years. In Fig. 3 the time after the eighth TP of the $3\,\mathrm{M}_\odot$ sequence with overshoot has been recalculated without overshoot at the bottom of the envelope convection. A profile at the beginning of the TDUP of the corresponding original sequence with overshoot is shown in Fig. 2. Close inspection and comparison with Fig. 3 shows that $10^{-4}\,\mathrm{M}_\odot$ of He-rich material have already been dredged-up. The additional mixing removes the sharp abundance discontinuity. This in turn dissolves the sharp discontinuity in the radiative gradient ∇_rad which sensitively depends on the opacity. In the envelope, hydrogen has a mass fraction of $\simeq 0.70$ and a higher opacity than helium. If this material is mixed into the stable region the radiative gradient will be lifted and dredge-up can occur.

This principle is not dependent on the efficiency of overshoot within a factor of maybe two (Fig. 13). At the lower edge of the AGB envelope the convective velocities are of the order of $\simeq 1\mathrm{km\,s^{-1}}$ while very efficient mixing at this convective boundary is still achieved by convective velocities down to $\leq 1\mathrm{cm\,s^{-1}}$. An instantaneously mixed region can be identified in which the downward directed flows decelerate from the initial velocity at the edge to the much lower velocity where the chemical abundance is not homogenized. Here, the turbulent velocity is so slow that mixing becomes inefficient. If the overshoot efficiency is small the region of homogenized composition may be very thin. This will still suffice to allow TDUP if the resolution is chosen such that overshoot is numerically able to smear out the abundance discontinuity (see below). Fig. 2 gives an impression of the masswise size of the overshoot region which can be barely identified in the abundance profiles on this scale. If the time steps are too large with a small overshoot, the smoothing effect on the abundance discontinuity is not efficient and DUP is prevented as is the case in the examples shown in Figs. 1b and Fig. 3.

In our calculations without overshoot ∇_rad and ∇_ad are first compared at each mass grid zone which defines stable and unstable grids. If a discontinuity has already built up, grids are included at the discontinuity in order to still resolve the abundance gradient. No mixing is allowed from an unstable grid to a stable grid. This approach closely realizes the MLT which predicts that no convective bubble can leave the convectively unstable region. However, one can argue equally well that the average of the gradients between neighboring grids should be compared. This criterion would allow material in stable grids to be mixed with material from the neighboring grid if the latter is unstable. Under certain conditions dredge-up may occur with the second treatment which would not occur with the first treatment.

During the dredge-up the upper part of the intershell region is engulfed by the convective envelope at the rate $\dot{M}_\mathrm{DUP} = \partial m_\mathrm{edge}/\partial t$ where m_edge is the mass coordinate of the convective boundary. Then, the extent ΔM_h (in Lagrangian coordinates) of the stable layer which is practically homogenized by extra mixing, depends on the overshoot efficiency and the rate $\dot{M}_\mathrm{DUP}$. ΔM_h is larger for a larger efficiency. Moreover, ΔM_h will be larger if $\dot{M}_\mathrm{DUP}$ is smaller and vice versa because element mixing is treated time dependently. With the efficiency $f = 0.016$ and $\dot{M}_\mathrm{DUP} \simeq 2 \cdot 10^{-5}\,\mathrm{M}_\odot/\,\mathrm{yr}$ we find $\Delta M_\mathrm{h} \simeq 10^{-6}\,\mathrm{M}_\odot$. In order to resolve the overshoot region the mesh size at and around the convective boundary should not exceed $\Delta M_\mathrm{h}/10$.

The time step is limited by the extent of the homogenized stable layer. Current stellar evolution calculations typically separate the solution of the structural equations and the solution of the mixing equations (often a diffusion-like equation) in order to save computational resources. This separated solution is justified if the two processes described by the two sets of equations operate on different time scales. If the numerical time step is of the order $\Delta t > \Delta M_\mathrm{h}/\dot{M}_\mathrm{DUP}$ then the mass coordinate of the envelope convection bottom m_edge after this time step would be below the previously homogenized layer: $m_\mathrm{edge}(t + \Delta t) < m_\mathrm{edge}(t) - \Delta M_\mathrm{h}$. In that case the separated solution of the structure equation and the equations of abundance change is no longer valid because the abundances

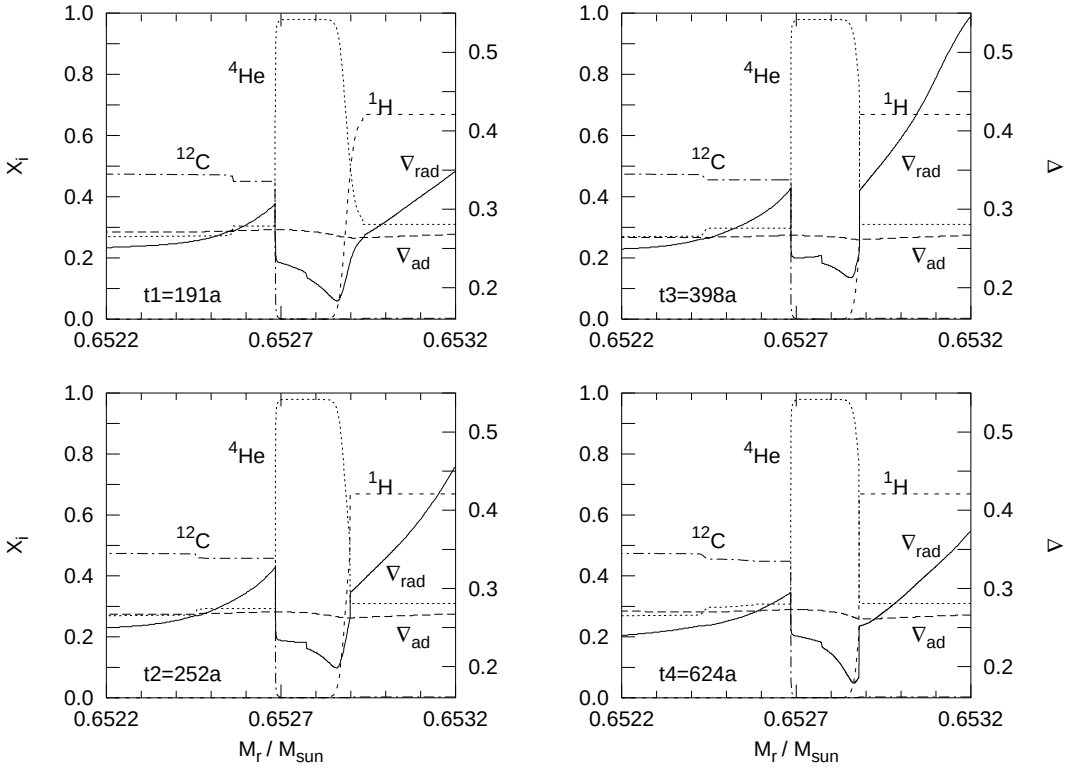

Fig. 3. A time series of the region of the former hydrogen-burning shell after the eighth TP of the $3\,\mathrm{M}_\odot$ sequence. The dredge-up phase after the thermal pulse of the overshoot sequence has been recalculated without overshoot and as a result dredge-up is prevented (compare Fig. 1) and Fig. 2. Abundances in mass fractions of ^{4}He (short-dashed), ^{12}C (dot-dashed) and hydrogen (dashed) refer to the left scale while the adiabatic ($\nabla_{\rm ad}$, long-dashed) and radiative ($\nabla_{\rm rad}$, solid line) temperature gradient refer to the right scale. For each panel the abscissa ranges from the bottom of the envelope at the right to the top of the intershell region at the left. In the middle of each panel a region of almost pure ^{4}He has been formed by hydrogen-burning during the previous interpulse phase. The lower boundary of the He-rich region is formed by the He-flash convection zone, which has at $t = 0\,\mathrm{yr}$ homogenized the intershell layers below $M_{\rm r} = 0.6527\,\mathrm{M}_\odot$. The four snapshots show how the bottom of the envelope convection zone advances downward by mass during the phase when TDUP would occur with overshoot. The order is from top to bottom and left to right and the ages are given with respect to the flash peak of the previous pulse. Note how the discontinuity of $\nabla_{\rm rad}$ is related to the abundance discontinuity which starts to build up ($t = 252\,\mathrm{yr}$). The discontinuity grows further ($t = 398\,\mathrm{yr}$) and finally when the region resumes contraction the bottom of the envelope convection retreats without being able to dredge-up material from the H-exhausted regions.

$Y(t + \Delta t)$ at $m_{\rm edge}(t + \Delta t)$ cannot be approximated by the abundances $Y(t)$. Only if this approximation is valid can the separate computation of structure and abundance change give correct results. This is only the case if $\Delta t < \Delta M_{\rm h}/\dot{M}_{\rm DUP}$.

The actual spatial resolution is controlled by a combination of criteria. Throughout the star we insert mass shells if any of the conditions $\Delta \log L > 0.01$, $\Delta \log P > 0.02$, $\Delta \log X(^{12}\mathrm{C}) > 0.02$ or $\Delta \log X(^{4}\mathrm{He}) > 0.02$ is fulfilled between two mass shells. After the He-flash, when the dredge-up is expected we increase the resolution in a region of about $0.06 \cdot \mathrm{M}_{\rm core}$ around the mass coordinate at the bottom of the envelope convection zone by requiring $\Delta \log P < 0.01$. This prescription for the spatial resolution ensures the above mentioned mesh size constraints in an adaptive way. Any further increase of resolution does not affect the amount of dredge-up obtained. Adapting the mesh may cause additional numerical diffusion. In the situation of the advancing convective boundary associated with the TDUP this does not prevent the discontinuity (Fig. 3) if no minimum grid size is enforced. However, numerical diffusion may easily distort the abundance profiles in the ^{13}C pocket (Fig. 4) when the grid density after the end of the TDUP is first reduced and then increases afterwards when H-burning starts.

4.2. The formation of the ^{13}C pocket and of an adjacent ^{14}N pocket

During the TDUP the hydrogen rich and convectively unstable envelope has contact with the radiative carbon rich intershell region. If the boundary of the envelope convection zone is treated according to the exponential diffusive overshoot method hydrogen diffuses into the carbon rich layer below. When the bottom of the envelope convection zone has reached the deepest position by mass, a region forms were protons from the envelope and ^{12}C from the intershell region coexist (Fig. 4, top panel). Note that the whole mass range shown in Fig. 4 is part of the overshoot region of the convective envelope. The solid line in the top panel shows the exponentially declining diffusion coefficient at the end of the dredge-up episode. In the right half of the panel D is large enough to cause a homogeneous element mixture. The profiles have developed cumulatively over a pe-

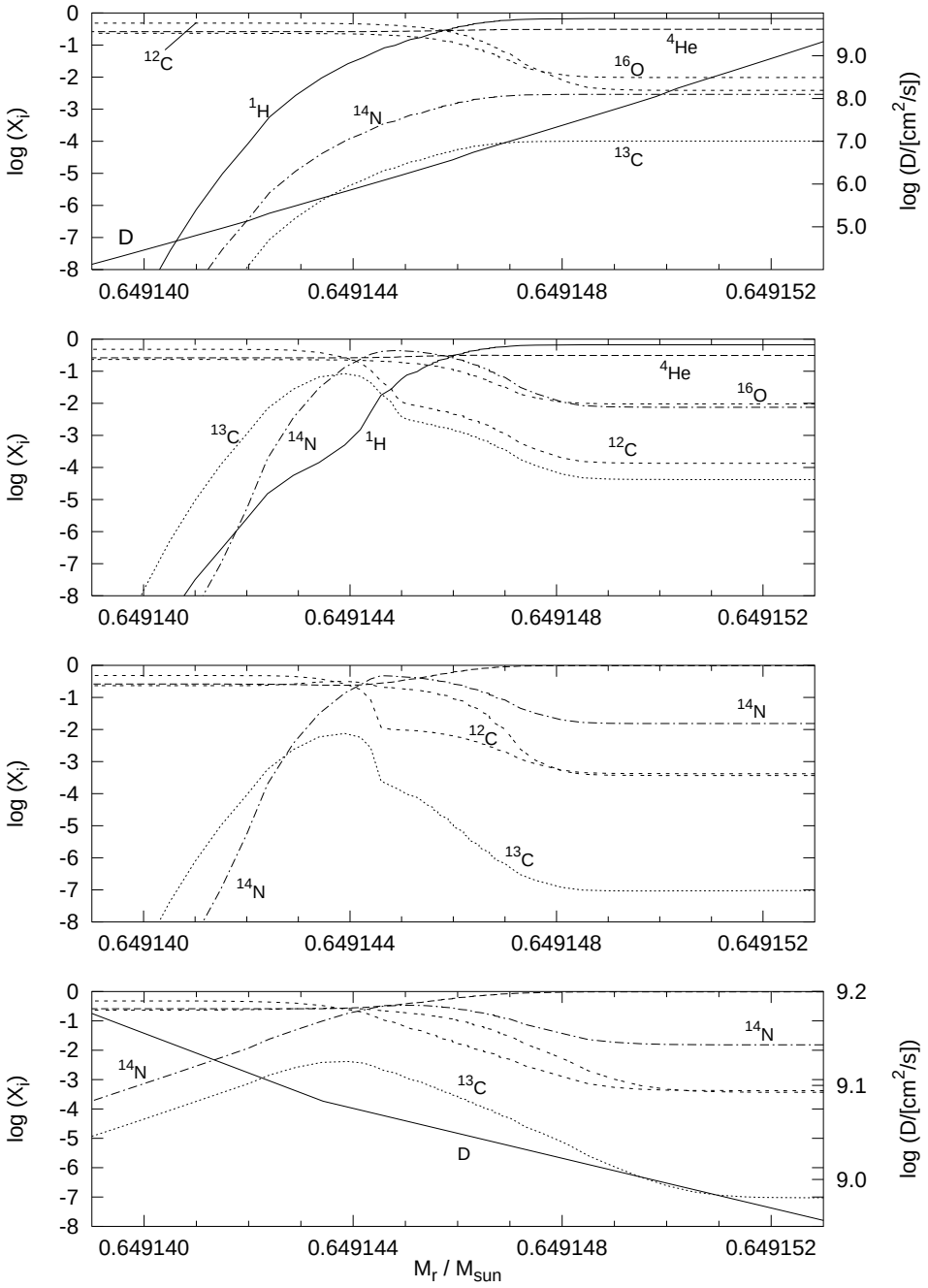

Fig. 4. Development and destruction of the ^{13}C pocket after the eighth TP of the $3\,M_\odot$ sequence. The panels show the abundance profiles of H,^{12}C and other isotopes in a mass range that contains the contact region of envelope and core at the end of the TDUP. The top panel shows a model after the end of the dredge-up episode (about $500\,$yr after the He-flash). The second panel shows a model about $1800\,$yr later when hydrogen burning has set in again. The third panel shows a model at the very end of the interpulse phase when ^{13}C has already been destroyed by reaction $^{13}\mathrm{C}(\alpha,n)^{16}\mathrm{O}$. The last panel shows the profiles at the onset of the next thermal pulse. The solid lines in the top and bottom panel are the diffusion coefficient (right scale) of these models. In the top panel the diffusion coefficient results from the overshoot of the envelope convection while in the bottom panel it is the diffusion coefficient of the upper overshoot zone of the He-flash convection zone during the ninth pulse.

riod of $\approx 50\,$yr during which the mass coordinate of the base of the envelope convection remains almost constant. In the left part the hydrogen abundance decreases as ^{12}C increases. Thus, the H/^{12}C number ratio decreases continuously from ~ 750 in the envelope to zero in the intershell region.

When the temperature increases during the succeeding evolution proton captures transform ^{12}C and H according to the continuously decreasing H/^{12}C ratio into a ^{13}C pocket and a prominent ^{14}N pocket side by side. The ^{13}C forms in the deeper layers where the H-abundance is below $\simeq 5\%$. Here the newly formed ^{13}C cannot be further processed into ^{14}N because all protons are already consumed. The ^{13}C abundance reaches a maximum mass fraction of 0.09 at $M_\mathrm{r} = 0.649144\,M_\odot$. Above this mass coordinate the H/^{12}C ratio is larger and after the formation of some ^{13}C there are still protons available which transform ^{13}C into ^{14}N. The ^{13}C/^{14}N ratio changes continuously in this region and at any position it is almost entirely determined by the initially present H/^{12}C ratio. Moreover, a ^{14}N pocket is a direct consequence of the continuous variation of the H and ^{12}C abundances from the core to the envelope. Therefore, if the efficiency of mixing is decreasing smoothly in the overshoot region a substantial ^{14}N pocket will inevitably form. The maximum abundance is given by the amount of ^{12}C in the intershell (see Sect. 5.2). In a narrow region (albeit larger than the region occupied by the ^{13}C pocket) ^{14}N becomes the most abundant isotope at a mass fraction of 0.45. The bend of the profile, e.g. at

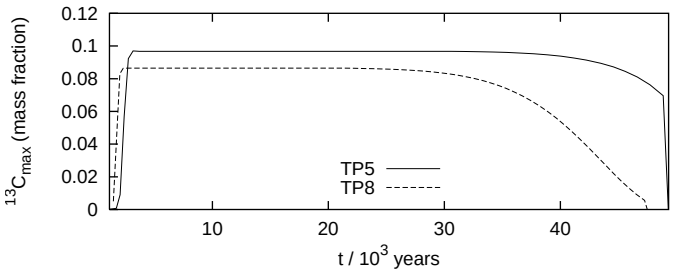

Fig. 5. The maximum ^{13}C abundance of the pocket after the fifth and eighth pulse of the $3\,M_\odot$ sequence displayed over one pulse cycle respectively. The zero time is set to the flash peak respectively.

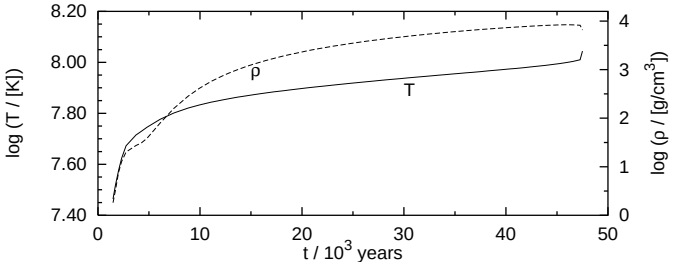

Fig. 6. The temperature and density at the location of the maximum ^{13}C abundance for the eighth TP corresponding to Fig. 5.

$M_{\rm r} = 0.649146\,M_\odot$ originates from the changing abundance ratios of ^{12}C, H and ^{14}N which are relevant for the production of ^{13}C.

Note that at the time when proton captures start to form the ^{13}C and ^{14}N pockets the radiative region *above* the burning region is well established. The isotopes made in this region cannot reach the surface at this time. Instead they are processed under radiative conditions (Straniero et al. 1995) and the products of this processing will be engulfed by the next He-flash convection zone. Thus, the production of ^{13}C after dredge-up with overshoot does not decrease the observed ^{12}C/^{13}C ratio in giant stars as suspected by Wallerstein & Knapp (1998).

During the whole interpulse period the region displayed in Fig. 4 is heating and contracting (Fig. 6). When the temperature has reached about $T = 10^8\,$K, ^{13}C is destroyed (Fig. 5) by $^{13}\mathrm{C}(\alpha,n)^{16}\mathrm{O}$ and neutrons are released. Towards the end of the interpulse period (third panel Fig. 4) most of the ^{13}C is burnt by α capture. The remaining small fraction is engulfed by the outwards reaching He-flash convection zone of the ninth pulse. This is displayed in the bottom panel of Fig. 4. The straight solid line shows the diffusion coefficient in the overshoot region at the top of this convection zone. Although the absolute value of D is larger than in the top panel, the impact on the abundance appears to be smaller. This effect is caused by the smaller velocity of the convective boundary of the envelope during the dredge-up compared to that of the boundary of the He-flash convection zone.

Fig. 5 shows that after more advanced pulses (like the eighth in this case), the ^{13}C formed at the hydrogen – carbon interface does indeed burn almost completely under radiative conditions (Straniero et al. 1995). The ^{13}C which formed after earlier pulses (like the fifth in this case) burns only partly under radiative conditions. After early thermal pulses a certain fraction of the ^{13}C will be mixed into the pulse-driven convective zone of the succeeding TP where it is processed under convective conditions in the intershell. In Fig. 6 the density and temperature at the position of the ^{13}C pocket are given for the case of the eighth TP. This shows the conditions under which the neutron capture operates.

With our overshoot description and assumption about the efficiency ($f = 0.016$) the layer in which the ^{13}C pocket forms is very thin (see Fig. 4). The total mass of ^{13}C contained in the pocket comprises only $\approx 2\ldots4\cdot10^{-7}\,M_\odot$. Estimates of the s-process element distribution from the ^{13}C neutron source demand that the pocket contains $\approx 1\ldots2\cdot10^{-5}\,M_\odot$ in order to model the main s-process component (Straniero et al. 1995). However, the numbers are not comparable at face value because the result of Straniero et al. is based on models without overshoot. Their hydrogen profile in the carbon rich region is not the same as our overshoot hydrogen profile. Also, the contribution and modification of the s-process element distribution from the $^{22}\mathrm{Ne}(\alpha,n)^{25}\mathrm{Mg}$ neutron source reaction during the high-temperature phase of the flash should be different in our models (see Sect. 5.1 and 6). Finally, the additional ^{14}N pocket which forms due to the overshoot model must be considered. On one hand ^{14}N is known to be an important neutron poison because of its large (n,p) cross section. On the other hand a large fraction of the neutrons lost by this reaction may be reproduced by $^{12}\mathrm{C}(p,n)^{13}\mathrm{N}(\beta^+)^{13}\mathrm{C}(\alpha,n)^{16}\mathrm{O}$. Moreover the additional amount of ^{14}N to be ingested into the next He-flash convection zone will also be converted into additional ^{22}Ne. All those processes will affect the s-process nucleosynthesis, which cannot be reduced to the mere amount of ^{13}C produced.

Preliminary tests with different overshoot efficiencies have shown that the shape of the abundance profiles in the region of the ^{13}C pocket is scaled with respect to the mass coordinate but conserved with respect to the abundance ratios. Intervals with certain mass ratios of, e.g. ^{12}C and hydrogen are just larger with a larger f. This means that a dedicated study of the s-process nucleosynthesis with a ^{13}C pocket according to our overshoot description should find that within a certain range of efficiencies the f-value does only determine the total amount of s-process elements in the dredged-up material but not its distribution. It should be investigated whether the functional form of an exponential velocity decay can reproduce a s-process distribution in compliance with the solar main component.

Apart from overshoot the process of rotationally induced mixing is a promising mechanism for the origin of the ^{13}C pocket (Langer et al. 1999). It is surprising that the overall amount of ^{13}C found in the pocket due to rotation is almost identical to the amount found here with overshoot (a few $10^{-7}\,M_\odot$).

5. The role of overshoot at the boundaries of the He-flash convection zone

During the He-flash the intershell region becomes convectively unstable due to the huge energy generation of the He-burning

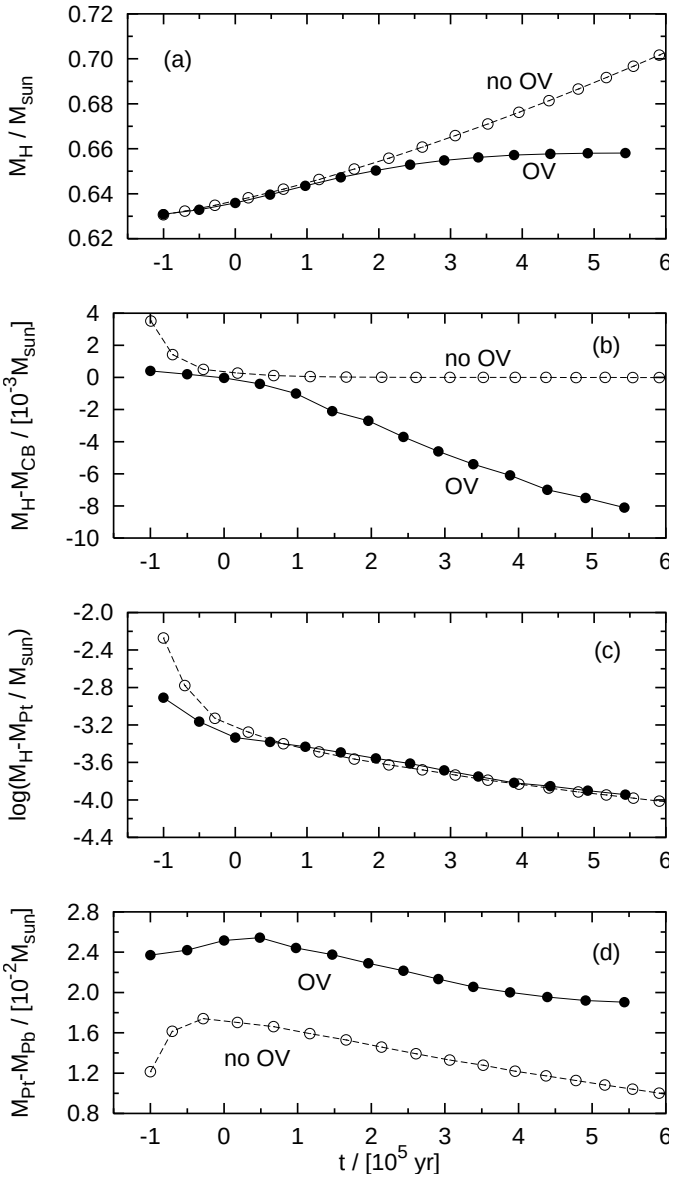

Fig. 7a–d. Evolution of the position and size in mass coordinates of several quantities at each TP as a function of time. Full symbols show the $3\,\mathrm{M}_\odot$ sequence computed with overshoot at all convective boundaries, open symbols represent the comparison sequence without any overshoot and started with the same initial model before the first TP as the $3\,\mathrm{M}_\odot$ sequence with overshoot. Panel **a**: H-free core at the TP, the increase by H-burning during the interpulse period is counterbalanced by the dredge-up after the TP for the overshoot sequence; **b**: difference of core mass at TP and smallest mass coordinate of convective envelope bottom achieved after the TP, negative values indicate DUP; **c**: difference of core mass at TP and the largest mass coordinate of the PDCZ top achieved during the TP, **d**: difference of top and bottom mass coordinate of PDCZ.

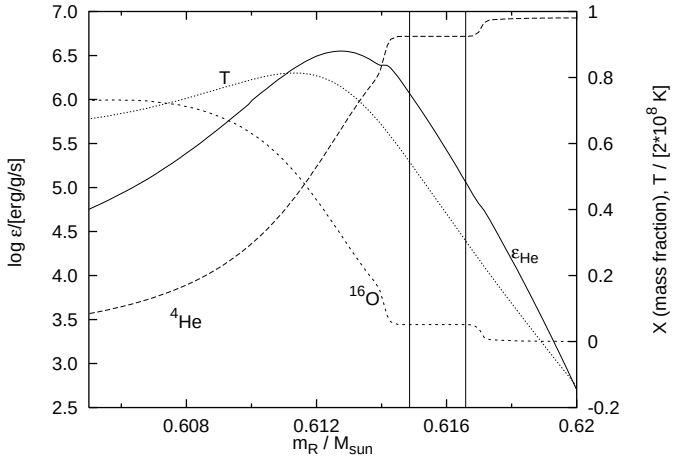

Fig. 8. Onset of He-flash convective instability in the intershell region at the first TP of $3\,\mathrm{M}_\odot$ sequence with overshoot. The two vertical lines show the upper (right) and lower (left) boundary of convection.

shell. Overshoot at the bottom of this He-flash convection zone leads to a deeper mixing from the region below the He-shell (the C/O core) into the intershell. This process could be called the fourth dredge-up (Iben 1999) or intershell dredge-up. Both the abundance in the intershell and also the structural parameters in the convection zone are affected by overshoot at the base of the He-flash convection zone. In particular, the change of the intershell abundance and the larger energy generation during the TP leads to very efficient TDUP (Herwig et al. 1999b). If these overshoot AGB models are used as starting models for the post-AGB evolution the long-standing discrepancy between observed surface abundances of H-deficient post-AGB stars and stellar models of this phase can be resolved (Herwig et al. 1999a).

5.1. Intershell structure during the flash

During the onset of the He-flash, when helium-burning increases rapidly, the layers just above the position of maximum energy generation and temperature become convectively unstable and the pulse-driven convection zone develops (Fig. 8). In this situation overshoot at the bottom of the PDCZ supplies additional fresh helium into the underlying nuclear burning region and supports the nuclear runaway. The situation is somewhat similar to hot-bottom burning were the hydrogen burning shell obtains additional nuclear fuel from the deep envelope convection and accordingly increases its energy production. Similarly the extra mixing below the PDCZ leads to a more violent He-flash with larger peak He-burning luminosities (Fig. 9) and larger mass $\Delta M_{\rm PDCZ}$ of the convectively unstable region (Fig. 7d). The stronger He-flashes are responsible for the structural and abundance consequences discussed below. The larger extent of the He-flash convection zone has immediate consequences, e.g. for the s-process nucleosynthesis: Heavy elements produced during the interpulse phase under radiative conditions are diluted in the convective intershell during the pulse before they are dredged-up into the envelope. For a larger He-flash convection zone the dilution effect will be larger.

Apparently there is no noticeable effect of overshoot at the top of the PDCZ. For the metallicity and overshoot efficiency considered here the minimum mass layer remaining between the

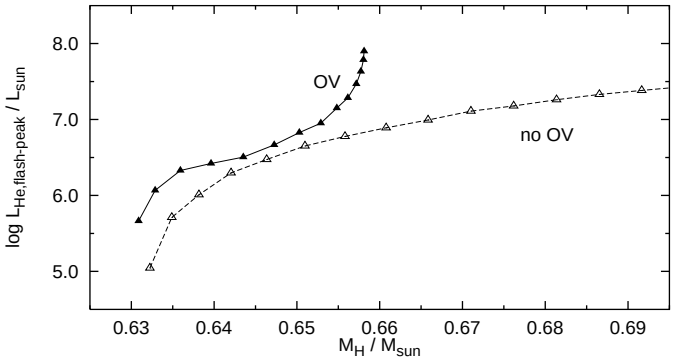

Fig. 9. The maximum helium-burning luminosities during the He-flash for the $3\,\mathrm{M}_\odot$ model sequence with (filled triangles) and without (open triangles) overshoot. Each symbol corresponds to one TP. The generally larger peak flash luminosities of the overshoot TPs are due to the extra-mixing below the bottom of the He-flash convection zone which leads to higher temperatures in the He-shell during the flash (Fig. 10). The relation runs vertically at $M_\mathrm{H} \simeq 0.657\,\mathrm{M}_\odot$ for the OV case because efficient dredge-up prevents further core mass growth ($\lambda \simeq 1$).

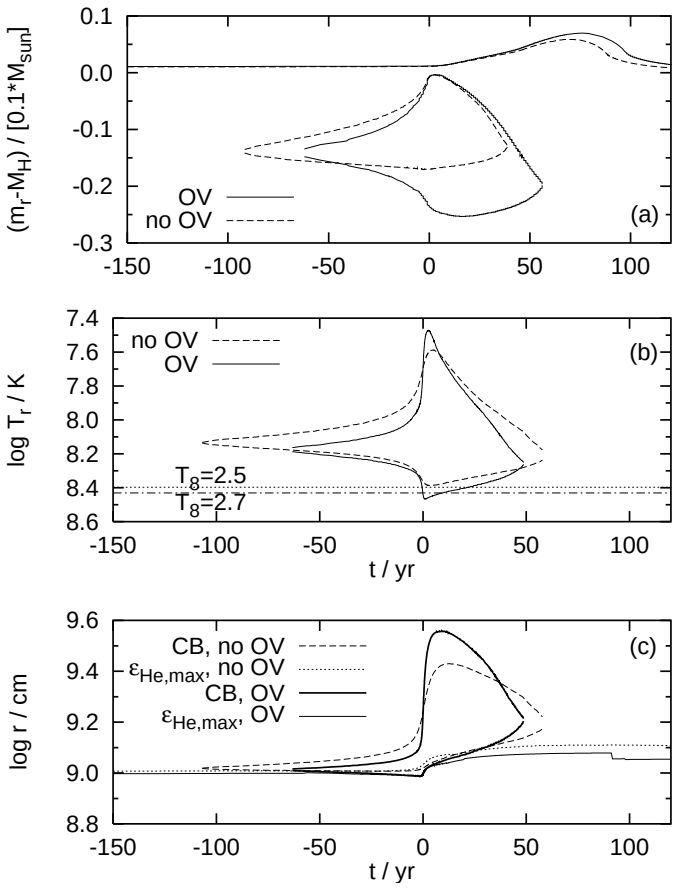

Fig. 10a–c. Panel **a**: The mass coordinates of the PDCZ boundary during the fifth TP of the $3.0\,\mathrm{M}_\odot$ with and without overshoot. The time has been set to zero at the moment where the He-burning luminosity has reached the maximum. Panel **b**: Temperature at the boundary of the He-flash convection zone of the same TP. Panel **c**: Geometric position of the PDCZ boundary (CB) and of the maximum energy release by helium burning.

H-rich envelope and the top of the PDCZ at its largest extension is independent on overshoot as can be seen from Fig. 7c.

The sequence without overshoot does not show any TDUP, and accordingly the whole intershell with the He-burning, and the H-burning shell at each boundary respectively is shifted outward by mass. For the $3\,\mathrm{M}_\odot$ sequence with overshoot dredge-up sets in at the third TP and the effective core mass growth ($\Delta M_\mathrm{H} - \Delta M_\mathrm{DUP}$) is slowed down (Fig. 7a,b). At the last computed TP of the $3\,\mathrm{M}_\odot$ sequence the intershell no longer evolves outward with mass. During this stationary shell burning the nuclear fuel for both the hydrogen and helium shell is transported downward by dredge-up. Over the pulse cycle the dredged-down hydrogen is first converted into helium which is then further mixed down by the He-flash convection zone. Finally the burning products are exchanged by dredge-up with fresh envelope material. In this situation dredge-up is not only important to mix processed material up but also to mix fresh material down and feed the stationary shells.

For the $4\,\mathrm{M}_\odot$ sequence the core mass actually decreases from pulse to pulse because $\lambda > 1$ (Table 2). In that case the nuclear burning shells are shifted inward with respect to mass. Obviously this situation can only last because fresh material for the nucleosynthesis is transported downward by dredge-up.

At the fifth TP ($3\,\mathrm{M}_\odot$) the core masses of the sequence with and without overshoot have not yet diverged too much due to the dredge-up difference between the two cases. However, the differences due to overshoot are already well established. Not only is the mass-wise extent of the PDCZ larger with overshoot (Fig. 7d) but in addition the convective instability is longer (Fig. 10a). The He-flash convection zone develops and disappears faster with overshoot. The overall duration of convective instability in the intershell is about $100\,\mathrm{yr}$ with overshoot and more than $150\,\mathrm{yr}$ for the case without overshoot.

With overshoot the temperature at the bottom of the He-flash convection zone is *larger* while at the top of the convectively unstable zone the temperature is *smaller* (Fig. 10b). Although the overall duration of the convective instability is larger without overshoot it is important to note that the high-T phase is much longer with overshoot. The duration of the high-T phase and the temperature reached during this phase is important for the analysis of the nucleosynthesis during the He-flash, in particular of the $^{22}\mathrm{Ne}$ neutron source ($^{22}\mathrm{Ne}(\alpha,\mathrm{n})^{25}\mathrm{Mg}$). Without overshoot the maximum temperature reached at the bottom of the He-flash convection zone during the fifth TP is $2.44 \cdot 10^8\,\mathrm{K}$. With overshoot the temperature at the bottom of the He-flash convection zone exceeds $2.5 \cdot 10^8\,\mathrm{K}$ for $21.8\,\mathrm{yr}$ while $T > 2.7 \cdot 10^8\,\mathrm{K}$ for $9.3\,\mathrm{yr}$. Over the following TPs the temperature in the He-flash convection will increase steadily. However, the general trend described above will remain preserved. Therefore, the exact mechanism of the s-process and also other aspects of the nucleosynthesis will be affected not only by the different intershell abundances due to overshoot but also because of different temperatures and time scales in the intershell during the He-flash.

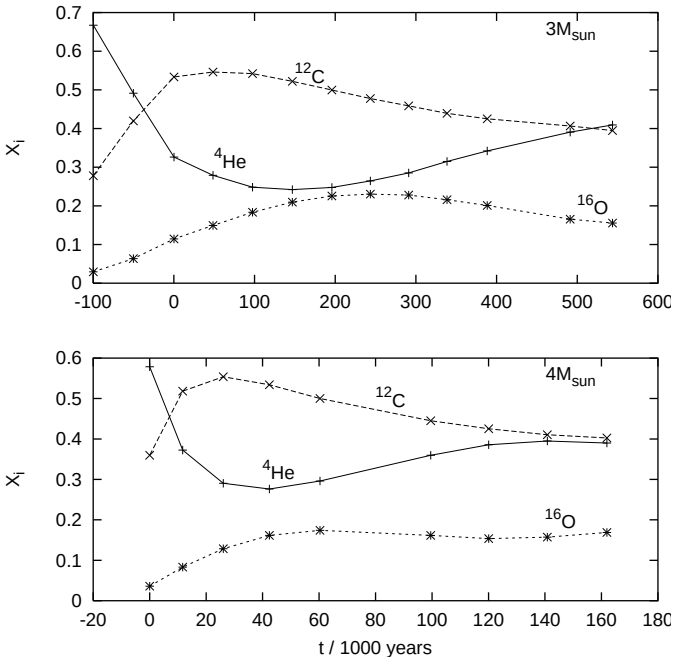

Fig. 11. Time evolution of abundances (mass fraction) in the upper part of the intershell shortly after each TP of the $3\,\mathrm{M}_\odot$ and $4\,\mathrm{M}_\odot$ model sequence with overshoot (compare with Boothroyd & Sackmann (1988a), Fig. 9). Each mark indicates one thermal pulse starting at the first TP. The zero point for the $3\,\mathrm{M}_\odot$ sequence has been set at the third TP where the TDUP stars.

Fig. 10c displays the geometric evolution of the He-flash convection zone together with the position of the maximum energy generation by helium burning. The fact that the temperature at the top of the He-flash convection zone is lower with overshoot is closely related to the greater expansion of the intershell in this case. With overshoot the largest geometric extent of the He-flash convection zone is about 1.4 times the distance found without overshoot.

5.2. The abundances in the intershell region

Models with overshoot have larger intershell mass fractions of carbon and oxygen at the expense of helium. In Fig. 11 the variation of the intershell abundances from pulse to pulse is shown. These models with overshoot show qualitatively the same dependence on the pulse number like models without overshoot (Schönberner 1979; Boothroyd & Sackmann 1988b) but the quantitative abundances are very different. During the first TPs the ^{12}C and ^{16}O abundance increases strongly at the expense of ^{4}He. After about six TPs the ^{4}He abundance in the intershell reaches a minimum while ^{12}C and ^{16}O go through a maximum. After about five to ten additional TPs all abundances are leveling at values which are similar to those found after the second or third TP. Quantitatively, overshoot with the efficiency $f = 0.016$ increases the amount of carbon by about a factor of two and the amount of oxygen by a factor of 10 to 20.

Test calculations in order to study the dependence of the intershell abundance on the efficiency of overshoot reveal that

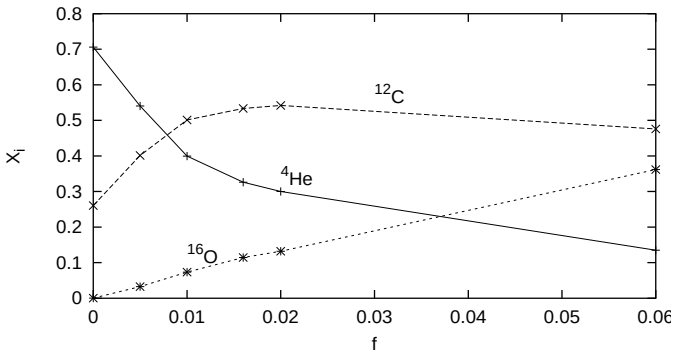

Fig. 12. Intershell abundances for different overshoot efficiencies after the third TP. Test model sequences have been calculated from the same starting model before the first TP with different values of f. The abundances for the sequence with $f = 0$ are computed without overshoot.

there is a relation between the overhoot parameter and the intershell abundance: larger overshoot leads to larger carbon and oxygen abundances and consequently smaller helium abundance. We have followed the evolution from the same starting model before the first TP over three TPs with different values of f. In Fig. 12 we display the abundance in the upper part of the intershell after the third TP. For $f = 0$ the abundances are the same as in Schönberner (1979). With larger and larger overshoot efficiency, the amount of oxygen increases almost linearly.

This correlation leads to a quite stringent constraint for the possible range for the overshoot efficiency f at the bottom of He-flash convection zone. We compare our intershell abundances with the surface abundances of the [WC]-type central stars of planetary nebulae (Koesterke & Hamann 1997; Hamann 1997; De Marco et al. 1998) and the PG 1159 stars (Dreizler & Heber 1998; Werner et al. 1999). The spectroscopic abundance analysis shows that these stars are very carbon rich and also oxygen rich. Typically, one finds (He,C,O)=(0.50,0.33,0.17) (mass fractions) for PG 1159 stars. Post-AGB stars become hydrogen-deficient because the intershell material appears at the surface in the aftermath of a very late TP (Herwig et al. 1999a). Thus, the observed surface abundances of H-deficient post-AGB stars must be interpreted as the intershell abundances of the progenitor AGB stars (Herwig & Blöcker 2000). Models without overshoot never show more than 2% of oxygen in the intershell and are thus unable to reproduce the large mass fraction of oxygen observed. This is a strong indication of the presence of at least some overshoot at the bottom of the He-flash convection zone. However, practically no H-deficient post-AGB stars are known to show more than about 20% of oxygen[2].

The oxygen abundances shown in Fig. 12 are an estimate of the surface oxygen abundance of a H-deficient post-AGB model evolved from the respective AGB model because the oxygen abundances after the third TP is already similar to the later TPs (Fig. 11). Any overshoot parameter much larger than $f = 0.03$ would lead to H-deficient post-AGB models with too large an oxygen abundance. Therefore, observations - together with the theoretical understanding of the evolutionary origin

[2] The exception, H1504+65, is free of H *and* He and has C $\simeq$ O.

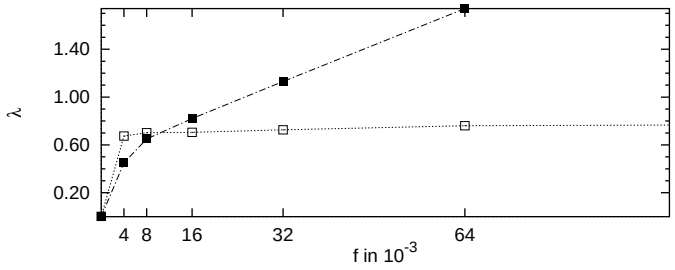

Fig. 13. Variation of the dredge-up efficiency λ with the overshoot efficiency. The open symbols represent cases where the f value has been changed just after the pulse-driven convective zone has disappeared after the eighth TP but before the bottom of the envelope convection has come close to the mass coordinate of the H-free core. Thus, in this case a different overshoot parameter is only effective at the bottom of the envelope during the dredge-up phase. The full symbols show the dredge-up efficiency after the following ninth TP which has been computed with the respective f-value also for the He-flash convection zone. In this case a different overshoot parameter has been effective at the bottom of the He-flash convection zone.

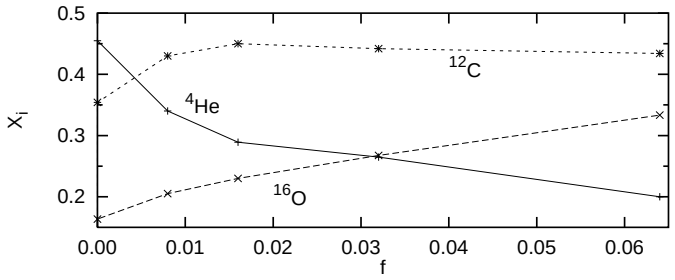

Fig. 14. The intershell abundances after the ninth TP as a function of f. While for Fig. 12 the different overshoot values have been applied over all previous TPs here we have computed only the ninth TP with different overshoot values. The starting model has been a $3\,\mathrm{M}_\odot$, $f = 0.016$ model before the ninth TP. This figure demonstrates how the abundances are modified due to overshoot during only one TP.

of H-deficient post-AGB stars - do constrain the overshoot efficiency at the bottom of the He-flash convection zone to a narrow range of $0.01 \lesssim f \lesssim 0.03$.

5.3. The third dredge-up and its dependence on overshoot at the bottom of the He-flash convection zone

One of the most important properties of TP-AGB models with overhoot is the efficient TDUP, which solves the problem of previous models to account for the typically low luminosities of carbon stars. In Table 1 and 2 the amount of dredged-up intershell mass and the related values for the dredge-up efficiency $\lambda = \Delta M_\lambda / \Delta M_{\rm H}$[3] are given for the $3\,\mathrm{M}_\odot$ and $4\,\mathrm{M}_\odot$ sequence with overshoot, and these results will be further discussed in Sect. 6.

Here, we consider the dependence of λ on the efficiency of overshoot. In particular it is important to clarify the different roles of overshoot below the bottom of the He-flash convection zone and below the bottom of the envelope convection zone (see also Sect. 4.1). For this purpose we have made a numerical experiment which involved the computation of one TP cycle with different values for the overshoot efficiency parameter f. The computations were started immediately after the He-flash convection zone of the eighth TP had disappeared. Thus, the dredge-up episode following this TP has been computed with different f values at the envelope convection zone only, while during the preceding TP f was the same for all convective boundaries. The resulting values for λ are shown in Fig. 13 as open symbols and demonstrate the dependence of the third dredge-up on the overshoot efficiency below the convective envelope. Within the considered range of f-values practically no dependence of λ on the overshoot efficiency exists. Only without any overshoot ($f = 0$) does dredge-up not occur for this TP. Even with f as small as 0.004 dredge-up is found with practically the same efficiency than with larger f (see Sect. 4.1). Note that the value of $\lambda \simeq 0.7$ displayed for the open symbols in Fig. 13 is just the value found for the eighth TP of the $3\,\mathrm{M}_\odot$ overshoot sequence (Table 1). If another TP had been chosen for this numerical experiment λ would have had the correspondingly larger or smaller value. Fig. 13 does not mean that models with overshoot applied only to the envelope convection always have $\lambda \simeq 0.7$.

The test model sequences have then been evolved beyond the dredge-up episode after the ninth TP. The respective f-values have now been applied to the convective boundaries of the He-flash convection zone as well. The resulting λ-values are represented by filled symbols in Fig. 13 and show the dependence of the dredge-up on the overshoot efficiency at the bottom of the He-flash convection zone. The full symbol at $f = 0.016$ shows $\lambda \simeq 0.8$, the value given in Table 1 for the ninth TP. f and λ are correlated: larger overshoot leads to larger dredge-up. The relation defined by the full symbols is specific to the chosen TP of this sequence. However, the trend is generally valid. A combination of effects is responsible for this correlation. With intershell overshoot the peak He-burning luminosities are substantially larger (Fig. 9). At the $14^{\rm th}$ TP of the overshoot sequence ($M_{\rm H} = 0.658\,\mathrm{M}_\odot$) the He-flash peak luminosity is $L_{\rm He} = 7.9 \cdot 10^7\,\mathrm{L}_\odot$. At the $14^{\rm th}$ TP of the sequence without overshoot ($M_{\rm H} = 0.692\,\mathrm{M}_\odot$) the peak luminosity is $L_{\rm He} = 2.4 \cdot 10^7\,\mathrm{L}_\odot$. Boothroyd & Sackmann (1988a) found for a $3\,\mathrm{M}_\odot$, Z=0.02 model sequence $L_{\rm He} \simeq 2 \cdot 10^7\,\mathrm{L}_\odot$ after about 20 TPs at a core mass $M_{\rm H} \simeq 0.65\,\mathrm{M}_\odot$. These models were computed without overshoot during the pre-AGB evolution and therefore have a lower core mass at the first TP $M_{\rm H1} \simeq 0.55\,\mathrm{M}_\odot$.

Greater He-flash strength leads to a greater expansion and cooling of the upper layers of the intershell (Fig. 10) and favors the occurrence of the TDUP ($\nabla_{\rm rad} \propto T^{-4}$). In Fig. 14 one can see that the modification of the intershell abundance during only one TP is considerable. The smaller He abundance with larger f leads to a larger opacity κ which favors the dredge-up also because $\nabla_{\rm rad} \propto \kappa$.

Thus the overshoot at the base of the He-flash convection zone strongly affects TDUP. In the previous section we have shown that f is constrained by the observational properties of

[3] λ = mass dredged-up after TP / growth of intershell by hydrogen burning during the preceding interpulse phase.

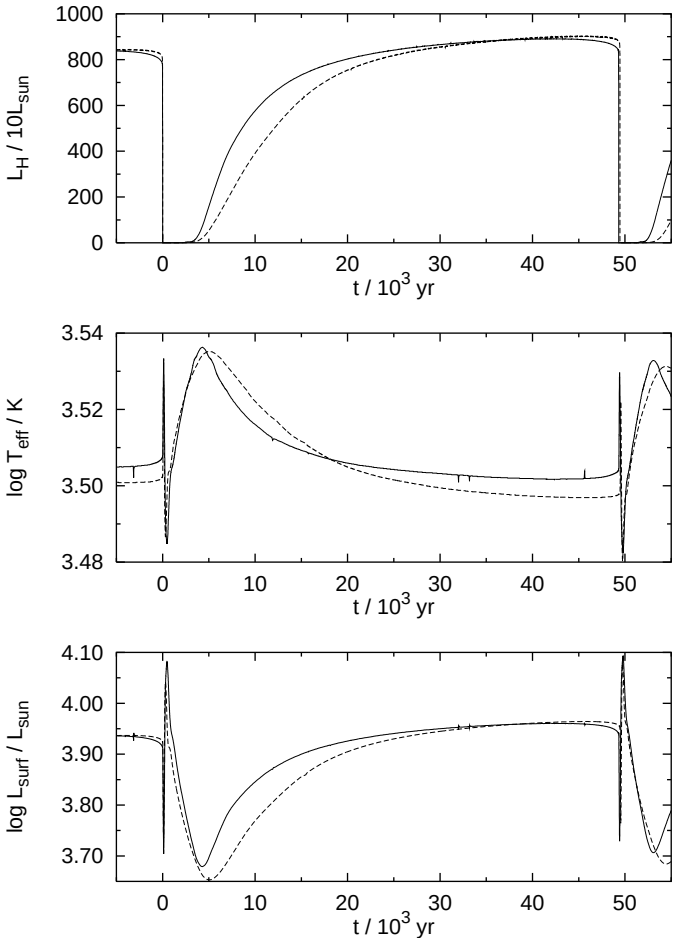

Fig. 15. Luminosity of H-burning (top panel), effective temperature (middle panel) and surface luminosity (bottom panel) for one complete pulse cycle of the sequence with (solid line) and without (dashed line) overshoot respectively. Time has been set to zero at the fifth TP.

H-deficient post-AGB stars. Therefore we conclude that the upper limit of the efficiency of TDUP can be constrained from observational properties of post-AGB stars.

6. Surface properties

In the previous sections we have described the different mechanisms by which overshoot influences the model properties. We will now focus on the surface properties of the models with overshoot.

Stellar parameters. The comparison of the core mass-luminosity relation of models with and without efficient dredge-up shows clear differences (Herwig et al. 1998). While models without dredge-up follow a linear relation when the asymptotic regime has been reached, models with very efficient dredge-up ($\lambda \simeq 1$) continue to increase in luminosity even if the core mass no longer increases. Here, the continuing radius decrease leads – according to simple homology relations (Refsdal & Weigert 1970) – to an increase in luminosities. This effect is most efficient over the earlier thermal pulses where the relative radius decrease per TP cycle is larger than after many thermal pulses when the core asymptotically resembles a white dwarf. The radius effect is responsible for the sub-luminous phase (compared to the luminosities expected from the core mass - luminosity relation) of the first few TPs, which is well known from any TP-AGB model sequence. However, the luminosity evolution continues to be strongly coupled to the core radius evolution. This becomes apparent only if the core mass is prevented from growing continuously in accordance with the radius shrinkage, as in models with efficient dredge-up. In addition, as Marigo et al. (1999) have pointed out, possibly up to one third of the luminosity increase observed by Herwig et al. (1998) can be ascribed to the well known effect of the molecular weight increase in the envelope as a result of dredge-up of processed material.

The rather short-term variation of the stellar parameters during and between the thermal pulses are affected as well. In general the surface luminosity reacts to the TP in the deep interior by a sudden ($\Delta t \simeq$ thermal timescale $\simeq 100\,\mathrm{yr}$) and drastic luminosity decline of about 40% of the pre-TP luminosity. It is followed (again on the thermal time scale) by an immediate luminosity jump which forms the more or less pronounced *TP surface luminosity peaks* (see Fig. 15 at $t = 0\,\mathrm{yr}$). The model sequence without overshoot shows only small TP-luminosity peaks after the first TPs with peak luminosities lower than the quiescent interpulse luminosity. Only after the third TP does the peak luminosity exceed the interpulse luminosity and over the following TPs the ratio of peak and interpulse luminosity grows. The model sequence with overshoot shows very large peaks already after the first TP with a ratio of ~ 1.6 between the peak and the interpulse luminosity which is gradually decreasing towards later TPs. At the fifth TP (Fig. 15) the surface luminosity peak is similar for the two sequences. The actual local He-luminosity peak during a TP is followed by a much smaller secondary peak. As this secondary maximum decays in the intershell the surface luminosity does also decline to the second surface luminosity minimum at $\sim 5000\,\mathrm{yr}$ in Fig. 15. Another difference caused by overshoot is a faster recovery of the H-burning shell after the TP (top panel Fig. 15). This is also reflected by the evolution of the surface parameters. For the model sequence with overshoot it takes only $\simeq 7600\,\mathrm{yr}$ from the TP until a 70% level of the previous interpulse luminosity at the surface has been regained while the sequence without overshoot requires $\simeq 11800\,\mathrm{yr}$. This effect is even more pronounced at later TPs, however it is then intermingled with the effect of different core mass evolution due to the different efficiency of the dredge-up.

Chemical evolution. The chemical evolution of AGB models with overshoot is different compared to models without overshoot due to four main effects:

1. The formation of a ^{13}C pocket in the upper part of the intershell region (Sect. 4.2). The consequences for the n-capture nucleosynthesis will be investigated elsewhere.
2. Substantially larger dredge-up, which leads to more efficient transport of processed material to the surface.

Table 1. Dredge-up properties of the thermal pulses of the $3\,M_\odot$ sequence with $f = 0.016$. The table gives the TP number, age (zero point set at first TP which shows dredge-up), peak luminosity of the helium burning shell $L_{\rm He}/\,L_\odot$, amount of dredged-up hydrogen free material $\Delta M_\lambda/\,M_\odot$, core growth since last TP $\Delta M_{\rm H}/\,M_\odot$, dredge-up parameter λ (see text), mass of hydrogen free core $M_{\rm H}$, mass coordinate of top of pulse-driven convective zone $M_{\rm Pt}$, mass coordinate of bottom of pulse-driven convective zone $M_{\rm Pb}$ and isotopic and elemental abundance ratios at the surface immediately after the TP.

TP	$\frac{\rm age}{\rm yr}$	$\frac{L_{\rm He}}{10^6\,L_\odot}$	$\frac{\Delta M_\lambda}{10^{-3}}$	$\frac{\Delta M_{\rm H}}{10^{-3}}$	λ	$\frac{M_{\rm H}}{M_\odot}$	$\frac{M_{\rm Pt}}{M_\odot}$	$\frac{M_{\rm Pb}}{M_\odot}$	$^{12/13}$C	C/O	$^{16/17}$O	$^{16/18}$O
1	−100079	0.46	–	–	–	0.63087	0.62969	0.60598	20.4	0.29	194.7	606.7
2	−50212	1.17	–	2.0	–	0.63288	0.63213	0.60795	″	″	″	″
3	1	2.13	0.03	3.1	–	0.63593	0.63547	0.61003	″	″	″	″
4	48519	2.63	0.4	3.7	0.10	0.63962	0.63920	0.61377	20.5	0.30	194.8	607.0
5	97563	3.18	1.0	4.3	0.23	0.64352	0.64315	0.61819	22.3	0.32	196.1	610.9
6	146883	4.63	2.1	4.7	0.44	0.64726	0.64694	0.62267	26.9	0.38	199.8	622.7
7	195842	6.71	2.7	5.1	0.53	0.65030	0.65002	0.62688	33.0	0.45	205.5	640.4
8	243582	8.80	3.7	5.3	0.71	0.65289	0.65265	0.63048	41.4	0.54	213.9	666.6
9	291084	13.9	4.6	5.7	0.82	0.65482	0.65461	0.63328	51.8	0.64	224.5	699.7
10	338588	19.0	5.4	6.0	0.91	0.65616	0.65598	0.63542	63.8	0.74	236.6	737.4
11	388433	29.4	6.1	6.4	0.98	0.65717	0.65702	0.63701	77.7	0.86	250.0	779.1
12	438979	42.9	7.0	6.8	1.02	0.65773	0.65759	0.63805	93.0	0.97	263.7	822.0
13	491151	59.9	7.5	7.3	1.04	0.65804	0.65804	0.63871	109.5	1.08	277.5	864.9

Table 2. Dredge-up properties of the thermal pulses of the $4\,M_\odot$ sequence with $f = 0.016$. For explanation of the displayed quantities see Table 1.

TP	$\frac{\rm age}{\rm yr}$	$\frac{L_{\rm He}}{10^6\,L_\odot}$	$\frac{\Delta M_\lambda}{10^{-3}}$	$\frac{\Delta M_{\rm H}}{10^{-3}}$	λ	$\frac{M_{\rm H}}{M_\odot}$	$\frac{M_{\rm Pt}}{M_\odot}$	$\frac{M_{\rm Pb}}{M_\odot}$	$^{12/13}$C	C/O	$^{16/17}$O	$^{16/18}$O
1	−80	2.26	2.39	–	–	0.78259	0.78239	0.77172	19.8	0.31	274.3	602.7
2	11660	3.70	3.12	1.91	1.63	0.78211	0.78192	0.77096	22.4	0.34	275.1	604.4
3	25990	6.21	3.94	2.61	1.51	0.78160	0.78144	0.77017	27.7	0.42	277.6	610.0
4	42350	11.5	4.79	3.17	1.51	0.78083	0.78070	0.76945	34.9	0.51	282.7	621.2
5	60290	21.0	5.41	3.58	1.51	0.77962	0.77953	0.76865	43.5	0.62	290.6	638.6
6	79610	38.1	5.63	3.93	1.43	0.77814	0.77806	0.76766	52.8	0.72	300.4	660.2
7	99500	59.8	5.90	4.16	1.42	0.77667	0.77661	0.76656	62.0	0.82	310.4	682.1
8	120030	92.6	5.92	4.45	1.33	0.77522	0.77517	0.76593	71.2	0.91	320.5	704.4
9	140790	123.3	0.61	4.59	1.33	0.77389	0.77384	0.76472	80.1	0.99	330.2	725.8
10	161900	142.6	0.64	4.74	1.37	0.77253	0.77248	0.76336	89.0	1.06	340.5	748.6
11	183480	195.5	0.65	4.92	1.32	0.77102	0.77128	0.76187	98.3	1.13	352.4	774.6

3. Higher temperature in He-flash convection zone during the TP (Fig. 10).
4. Depletion of helium and larger ^{16}O and ^{12}C abundance in the intershell due to deeper penetration of the bottom of the He-flash convection zone into the C/O-core.

These effects are reflected by the chemical evolution at the stellar surface (Table 1 and 2).

C/O and carbon isotopic ratio. Recurring and efficient dredge-up transports primary ^{12}C into the envelope after each TP. ^{13}C is not produced or destroyed in the stars of the mass range discussed here. This leads to a steady increase of the ^{12}C/^{13}C ratio at the surface. At the same time also the C/O ratio increases from its initial value of ~ 0.3 and exceeds unity after a number of TPs. Note that in calculations with overshoot ^{16}O is also mixed into the envelope at each dredge-up event. Because of this additional ^{16}O the C/O ratio grows more slowly with overshoot than without overshoot if λ where the same. However, this effect is more than compensated for by two other effects: the dredge-up itself is larger and the mass fraction of ^{12}C and ^{16}O of the dredged-up intershell material is larger. This leads to a larger increase of the C/O ratio for each TP. For example, as can be seen from Table 2 the $4\,M_\odot$ sequence becomes C-rich at the tenth TP contrary to the results of Forestini & Charbonnel (1997) and Marigo et al. (1996) who both find that a $4\,M_\odot$ AGB star of solar metallicity does not become a C-star at all. Note that these authors assume dredge-up to operate and that HBB cannot prevent a $4\,M_\odot$ star from getting C-rich.

Fig. 16 compares observational data of the chemical composition of AGB stars with the model data of the sequences with overshoot. The filled symbols in the lower left corner correspond to the first TPs. The observational data shows properties of M- S- and C-giant[4] stars with different masses (most of them smaller than those of the model sequences) which presumably also have experienced a different number of TPs.[5] However, apart from

[4] M-giants:C/O $<$ 0.8, S-giants: 0.8 $<$ C/O $<$ 1.0, C-giants:C/O $>$ 1.0.

[5] Giants without Tc have been excluded from Fig. 16 because their abundance anomaly might be due to transfer of mantle material from a companion (Habing 1996).

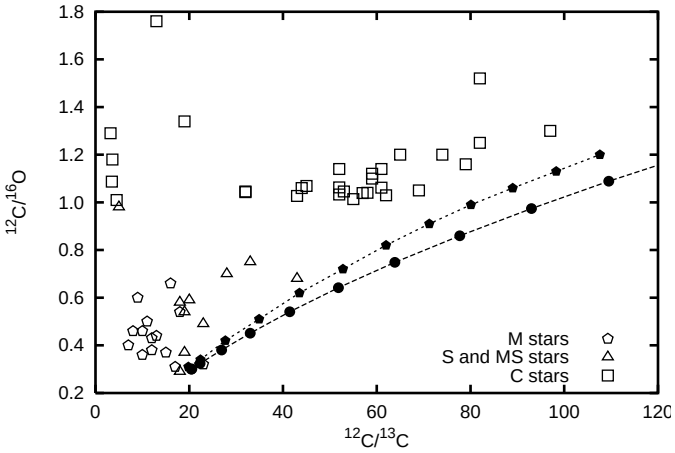

Fig. 16. Reproduction of $^{12}C/^{16}O$ versus $^{12}C/^{13}C$ plot in Smith & Lambert (1990) (open symbols) together with the surface ratios of the $3\,M_\odot$ (filled circles) and $4\,M_\odot$ (filled pentagons) model sequence. See text for details.

giants with $C/O \approx 1$ and very low $^{12}C/^{13}C$ ratio (J-giants), a correlation between the two ratios is apparent. With respect to the model data this correlation must be interpreted as a time evolution. The model sequences do generally follow the observed trend. However, the theoretical relation shows an offset to the observations and also a somewhat smaller slope. In addition the increment of the ratio from TP to TP is rather large and depending on mass loss several more TP are likely for these model sequences, leading to very large $^{12}C/^{13}C$ ratios. A somewhat smaller overshoot efficiency would result in a lower dredge-up efficiency and a smaller amount of dredged-up oxygen. While the first effect would decrease the steps at which the model sequence passes along the diagram, the latter would increase the slope of the theoretical relation somewhat. As another detail, the initial abundance ratios have a considerable influence on the theoretical prediction. Most of the displayed stars are probably of lower mass and therefore their initial $^{12}C/^{13}C$ ratio before the first TP was closer to ~ 10 (Gilroy 1989) than around 20. This initial $^{12}C/^{13}C$ ratio determines the the slope of the $^{12}C/^{13}C$ - C/O relation as well, with a smaller initial ratio leading to a larger slope. Thus, models with initial masses around or below $2\,M_\odot$ should show a larger slope due to this effect and should show a better agreement with the observations.

Oxygen isotopic ratios. Observationally the oxygen isotopic ratios $^{16}O/^{17}O$ and $^{16}O/^{18}O$ of AGB stars extend to much larger values than predicted by evolutionary models. Theoretical models without overshoot cannot account for increasing $^{16}O/^{17}O$ and $^{16}O/^{18}O$ ratios because dredge-up is only achieved with difficulty for the relevant masses. Even if this problem is circumvented by assuming dredge-up to be present then the dredged-up material leads only to a rather inefficient dilution of ^{17}O and ^{18}O in the envelope because the dredged-up material is depleted in these isotopes compared to the envelope value. The ^{16}O abundance in the intershell of models without overshoot is similar to the envelope abundance and no modification can be expected there.

Harris et al. (1985; 1987) determined for $^{16}O/^{17}O$ and $^{16}O/^{18}O$ values between 600 and 3000. It is also interesting to note that the two ratios are correlated. Moreover, both ratios seem to be correlated with the neutron exposure associated with the observed s-process abundances and also with the carbon abundance. Both, an increasing carbon abundance and an increasing neutron exposure are indicating more efficient or more frequent dredge-up because s-process elements and carbon are not made in or at the bottom of the envelope. It is therefore likely that the enormous oxygen isotopic ratios are related to the TDUP.

Forestini & Charbonnel (1997) have assumed dredge-up and predict from an extrapolation of their models without overshoot an increase of the $^{16}O/^{17}O$ ratio of 13% (2%) from initially ~ 320 for the entire AGB evolution of their solar $3\,M_\odot$ ($4\,M_\odot$) case and almost the same values for the $^{16}O/^{18}O$ ratio starting from initially ~ 600. The evolutionary effect in the overshoot model is significantly larger because the abundance of ^{16}O in the dredged-up material is five to ten times larger if overshoot is considered compared to models without overshoot. Over the first dozen TPs available in Table 1 and 2, the oxygen isotopic ratios increase by about 44% (28%) for the $3\,M_\odot$ ($4\,M_\odot$) case. Similar to what has been said previously a comparison of absolute numbers observed to the model predictions is misleading at this stage. The initial model $^{16}O/^{17}O$ ratios are probably too small, possibly due to a wrong $^{17}O(p,\alpha)$ reaction rate. Also, most of the observed data will belong to less massive stars for which comparable model data do not yet exist. Clearly, this issue needs a more detailed investigation. However, it seems that overshoot can contribute to the solution of this problem.

Magnesium isotopic ratios. The evolution of the magnesium isotopic ratios $^{24}Mg/^{25}Mg$ and $^{24}Mg/^{26}Mg$ are not only tracers of the TDUP but also of the temperature in the He-burning shell during the thermal pulses. While ^{24}Mg is not produced or destructed in AGB stars the other Mg isotopes are produced during the TP by α captures of ^{22}Ne. The latter is abundant in the intershell as a result of two α captures on ^{14}N. Since the temperature at the bottom of the He-flash convection zone is larger if overshoot is present (Fig. 10) the reactions $^{22}Ne(\alpha,n)^{25}Mg$ and $^{22}Ne(\alpha,\gamma)^{26}Mg$ are more efficient. The $3\,M_\odot$ ($4\,M_\odot$) sequence accordingly shows a decrease of $^{24}Mg/^{25}Mg$ from 8.0 (8.1) at the first TP to 4.9 (3.9) at the last TP computed. The $^{24}Mg/^{26}Mg$ ratio is 7.1 (7.0) for the $3\,M_\odot$ ($4\,M_\odot$) sequence at the first TP and decreases to 5.8 (5.3) at the last computed TP (see previous tables). Again, this decrease for the first dozen TP is stronger than that predicted by Forestini & Charbonnel (1997) for the entire evolution.

7. Conclusions

We have studied how the evolution of AGB stars is affected by exponential diffusive overshoot at all convective boundaries.

The main differences between models with overshoot compared to models without overshoot are

1. – a depletion of helium and enhancement of carbon and oxygen in the intershell abundance distribution which is caused by,
   – a deeper penetration of the He-flash convection zone into the C/O core below (intershell or fourth dredge-up),
2. – larger energy generation by He-burning during the thermal pulse and consequently,
   – higher temperature at the bottom of the He-flash convection zone and lower temperature at the top,
3. – substantially increased dredge-up of material which has a modified abundance distribution compared to models without overshoot and as a result,
   – a different evolution of the surface abundances showing a stronger signature of nucleosynthesis and
   – a constant or decreasing core mass during some more advanced TPs,
4. – a faster recovery of the hydrogen-burning shell after the TP and correlated with this,
   – a faster recovery of the surface abundance after the TP compared to models without overshoot, and
5. the formation of a ^{13}C and a ^{14}N pocket at the envelope-core interface at the end of the dredge-up.

These properties of AGB evolution models improve the understanding of observationally obtained information about AGB stars. To date no obvious contradictions of observational properties and AGB models with overshoot have appeared. On the other hand, overshoot in AGB stellar models (in particular that at the base of the He-flash convection zone) has been an indispensable precondition for the starting point of H-deficient post-AGB model sequences which can explain the observed abundance ratios of these stars, in particular their oxygen abundance (Herwig et al. 1999a). Therefore, overshoot should be considered an important ingredient for the modeling of AGB stars.

Acknowledgements. This work has been supported by the *Deutsche Forschungsgemeinschaft, DFG* (grants Scho 394/13 and La 587/16). I greatly appreciate previous improvements to the evolution code and stimulating support by T. Blöcker. Further more I would like to thank R. Gallino, L. Koesterke, N. Langer and D. Schönberner for advice, helpful discussions and proof reading. The referee, A. Bressan, is acknowledged for his very useful comments.

References

Alongi M., Bertelli G., Bressan A., Chiosi C., 1991, A&A 244, 95
Alongi M., Bertelli G., Bressan A., et al., 1993, A&A 97, 851
Anders E., Grevesse N., 1989, Geochim. Cosmochim. Acta 53, 197
Andersen J., Nordström B., Clausen J.V., 1990, ApJ 363, L33
Aparicio A., Bertelli G., Chiosi C., Garcia-Pelayo J.M., 1991, A&AS 88, 155
Blöcker T., 1995, A&A 297, 727
Blöcker T., Herwig F., Driebe T., 2000, In: D'Antona F., Gallino R. (eds.) The changes in abundances in AGB stars. Mem. Soc. Astron. Ital., in press, astro-ph/0002455
Blöcker T., Herwig F., Schönberner D., Eid M.E., 1997, In: The Carbon Star Phenomenon. IAU Symp. 177, Antalya, Turkey, in press
Böhm-Vitense E., 1958, Z. Astrophys. 46, 108
Boothroyd A.I., Sackmann I.-J., 1988a, ApJ 328, 653
Boothroyd A.I., Sackmann I.-J., 1988b, ApJ 328, 671
Bressan A., Fagotto F., Bertelli G., Chiosi C., 1993, A&AS 100, 647
Bressan A.G., Bertelli G., Chiosi C., 1981, A&A 102, 25
Canuto V.M., 1998, ApJ 508, L103
Caughlan G.R., Fowler W.A., 1988, Atom. Data Nucl. Data Tables 40, 283, CF88
D'Antona F., Mazzitelli I., 1996, ApJ 470, 1093
De Marco O., Storey P.J., Barlow M.J., 1998, MNRAS 297, 999
Deng L., Bressan A., Chiosi C., 1996a, A&A 313, 145
Deng L., Bressan A., Chiosi C., 1996b, A&A 313, 159
Dreizler S., Heber U., 1998, A&A 334, 618
El Eid M., 1994, A&A 285, 915
Forestini M., Charbonnel C., 1997, A&AS 123, 241
Freytag B., Ludwig H.-G., Steffen M., 1996, A&A 313, 497
Frogel J.A., Mould J., Blanco V.M., 1990, ApJ 352, 96
Frost C.A., Lattanzio J.C., 1996, ApJ 473, 383
Gallino R., Arlandini C., Busso M., et al., 1998, ApJ 497, 388
Gallino R., Busso M., Lugaro M., 1997, In: Bernatowitz T., Zinner E. (eds.) Astrophysical Implications of the Laboratory Study of Presolar Materials. AIP Conf. Ser., p. 115
Gilroy K.K., 1989, ApJ 347, 835
Habing H.J., 1996, A&AR 7, 97
Hamann W.-R., 1997, In: Habing H., Lamers H. (eds.) Planetary Nebulae. IAU Symp. 180, Kluwer, p. 91
Harris M.J., Lambert D.L., Hinkle K.H., Gustafsson B., Eriksson K., 1987, ApJ 316, 294
Harris M.J., Lambert D.L., Smith V.V., 1985, ApJ 299, 375
Herwig F., Blöcker T., 2000, In: The galactic Halo: From Globular Clusters to Field Stars. Proc. of the 35nd Liège Int. Astr. Coll., Universtité de Liège, in press
Herwig F., Blöcker T., Driebe T., 2000, In: D'Antona F., Gallino R. (eds.) The changes in abundances in AGB stars. Mem. Soc. Astron. Ital., in press, astro-ph/9912350
Herwig F., Blöcker T., Langer N., Driebe T., 1999a, A&A 349, L5, HBLD99
Herwig F., Blöcker T., Schönberner D., 1999b, In: Bertre T.L., Lebre A., Waelkens C. (eds.) AGB Stars. IAU Symp. 191, p. 41
Herwig F., Blöcker T., Schönberner D., El Eid M.F., 1997, A&A 324, L81
Herwig F., Schönberner D., Blöcker T., 1998, A&A 340, L43
Hollowell D., Iben Jr. I., 1988, ApJ 333, L25
Hurlburt N.E., Toomre J., Massaguer J.M., 1986, ApJ 311, 563
Hurlburt N.E., Toomre J., Massaguer J.M., Zahn J.-P., 1994, ApJ 421, 245
Iben Jr. I., 1975, ApJ 196, 525
Iben Jr. I., 1976, ApJ 208, 165
Iben Jr. I., 1977, ApJ 217, 788
Iben Jr. I., 1999, In: Bertre T.L., Lebre A., Waelkens C. (eds.) AGB Stars. IAU Symp. 191, p. 591
Iben Jr. I., Renzini A., 1983, ARA&A 21, 271
Iben Jr. I., Truran J.W., 1978, ApJ 220, 980
Iben Jr. I., Tutukov A.V., Yungelson L.R., 1996, ApJ 456, 750
Iglesias C.A., Rogers F.J., 1996, ApJ 464, 943
Kippenhahn R., Weigert A., 1990, Stellar structure and evolution. Springer, Berlin
Koesterke L., Hamann W.R., 1997, A&A 320, 91

Kozhurina-Platais V., Demarque P., Platais I., Orosz J.A., Barnes S., 1997, AJ 113(3), 1045
Landré V., Prantzos N., Aguer P., et al., 1990, A&A 240, 85
Langer N., 1986, A&A 164, 45
Langer N., El Eid M., Fricke K.J., 1985, A&A 145, 179
Langer N., Fricke K.J., Sugimoto D., 1983, A&A 126, 207
Langer N., Heger A., Wellstein S., Herwig F., 1999, A&A 346, L37
Lattanzio J.C., 1986, ApJ 311, 708
Lattanzio J.C., 1989, ApJ 344, L25
Lattanzio J.C., Boothroyd A.I., 1997, In: Bernatowitz T., Zinner E. (eds.) Astrophysical Implications of the Laboratory Study of Presolar Materials. AIP Conf. Ser., p. 85
Maeder A., 1975, A&A 40, 303
Maeder A., Meynet G., 1989, A&A 210, 155
Marigo P., Bressan A., Chiosi C., 1996, A&A 313, 545
Marigo P., Girardi L., Weiss A., Groenewegen M.A.T., 1999, A&A 351, 161, in press
Mazzitelli I., D'Antona F., Ventura P., 1999, A&A 348, 846
Mermilliod J.C., Maeder A., 1986, A&A 158, 45
Mowlavi N., 1999, A&A 344, 617
Napiwotzki R., Schönberner D., Weidemann V., 1991, A&A 243, L5
Paczyński B., 1977, ApJ 214, 812
Pinsonneault M., 1997, ARA&A 35, 557
Refsdal S., Weigert A., 1970, Z. Astrophys. 6, 426
Renzini A., 1987, A&A 188, 49
Roxburgh I.W., 1978, A&A 65, 281
Sackmann I.J., 1980, ApJ 241, L37
Salasnich B., Bressan A., Chiosi C., 1999, A&A 342, 131
Schaller G., Schaerer D., Meynet G., Maeder A., 1992, A&AS 96, 269
Schönberner D., 1979, A&A 79, 108
Schönberner D., 1996, In: Jeffery C.S., Heber U. (eds.) Hydrogen-Deficient Stars. ASP Conf. Series Vol. 96, p. 433
Schröder K.-P., Pols O.R., Eggleton P., 1997, MNRAS 285, 696
Schwarzschild M., Härm R., 1965, ApJ 142, 855
Shaviv G., Salpeter E., 1973, ApJ 184, 191
Smith V.V., Lambert D.L., 1990, ApJS 72, 387
Smith V.V., Lambert D.L., McWilliam A., 1987, ApJ 320, 862
Stein R.F., Nordlund A., 1998, ApJ 499, 914
Stothers R., 1991, ApJ 383, 820
Straniero O., Chieffi A., Limongi M., et al., 1997, ApJ 478, 332
Straniero O., Gallino R., Busso M., et al., 1995, ApJ 440, L85
Vassiliadis E., Wood P., 1993, ApJ 413, 641
Ventura P., Zeppieri A., Mazzitelli I., D'Antona F., 1998, A&A 334, 953
Wagenhuber J., Groenewegen M.A.T., 1998, A&A 340, 183
Wallerstein G., Iben Jr. I., Parker P., et al., 1997, Rev. Mod. Phys. 69(4), 995
Wallerstein G., Knapp G.R., 1998, ARA&A 36, 369
Weaver T.A., Woosley S.E., 1993, Physics Reports 40(227), 65
Weidemann V., 2000, A&A, submitted
Weigert A., 1966, Z. Astrophys. 64, 395
Werner K., Dreizler S., Rauch T., Koesterke L., Heber U., 1999, In: Bertre T.L., Lebre A., Waelkens C. (eds.) AGB Stars. IAU Symp. 191, p. 493
Wood P.R., 1981, In: Iben I Jr., Renzini A. (eds.) Physical Processes in Red Giants, p. 135
Xiong D.R., 1985, A&A 150, 133
Zuckerman B., Aller L.H., 1986, ApJ 301, 772